On the Nature of the Trigonal Fields in Hexaaquachromium(III) in Guanidinium Aluminum Sulfate Hexahydrate

H. Riesen*

University College, The University of New South Wales, Australian Defence Force Academy, Canberra, ACT 2600, Australia

L. Dubicki

Research School of Chemistry, The Australian National University, Canberra, ACT 0200, Australia

Received December 21, 1999

Zeeman and site selective luminescence and excitation spectra in the region of the $^2E \leftarrow {}^4A_2$ transition are reported for the hexaaquachromium(III) complex in the trigonal ferroelectric guanidinium aluminum sulfate hexahydrate. The two prominent transitions are due to the R_1 lines of the two sites of C_3 and C_{3v} point symmetry. The two R_1 lines display $g_{||} = -3.1$ and $g_{||} = -3.2$, respectively, and show no measurable Zeeman shift or splitting with B⊥c. This behavior is consistent with the presence of a very large trigonal field. A peculiar feature of the present system is the conspicuous absence of any prominent R_2 line. From the Zeeman data with B⊥c and a comparison of vibrational sidelines in excitation and luminescence it is concluded that the R_2 level strongly interacts with vibrational levels.

Introduction

Hexaaqua complexes of transition metals are archetypal coordination compounds and have attracted wide interest by inorganic chemists over many decades. A very interesting feature of hexaaqua complexes is the sensitivity of the electronic structure to the orientation of the H_2O molecules.

Guanidinium aluminum sulfate hexahydrate, $C(NH_2)_3Al(SO_4)_2 \cdot 6H_2O$, abbreviated as GAlSH, and its chromium(III) analogue (GCrSH) have been extensively investigated because of their ferroelectric behavior.[1−5]

In an early spectroscopic study[6,7] of GCrSH and GAlSH:Cr(III) the two prominent electronic features in the region of the $^2E(2\bar{A},\bar{E}) \leftarrow {}^4A_2$ transition were assigned to the $R_1(\bar{E})$ lines of the two crystallographically inequivalent sites of C_3 and C_{3v} symmetry. This interpretation was later challenged, and the two lines were reassigned to the $R_1(\bar{E})$ and $R_2(2\bar{A})$ transitions of one site.[8] The main argument in this latter work was the surprising absence of the R_2 line if the two prominent transitions were attributed to the R_1 lines of two crystallographically inequivalent sites.

However, the original Zeeman studies[6,7] were correct and later Zeeman experiments[9] confirmed the original assignments. For neat GCrSH at 4.2 K, the two sharp lines R at 14 111 cm^{-1} and R' at 14 131 cm^{-1} correspond to species with a ground-state zero field splitting (ZFS) of 0.14 and 0.18 cm^{-1}, respectively.[7,9] The ZFS is defined as $D(^4A_2) = E(\pm 1/2) - E(\pm 3/2)$. The unit cell of GAlSH or GCrSH contains two inequivalent sites of C_3 and C_{3v} symmetry with a population of 2 and 1, respectively. Subsequent EPR studies[10] of GGaSH:Cr^{3+} identified the species with the ZFS = 0.14 and 0.18 cm^{-1} to be the C_3 and C_{3v} sites, respectively.

The problem of identifying the second origin $R_2(2\bar{A})$ has not been resolved, and hence the magnitude of the trigonal field v is not known. The trigonal field v is diagonal within the t_{2g} orbitals and $v = E(t_{2xo}) - E(t_{2x\pm})$, where t_{2xo} and $t_{2x\pm}$ are the complex trigonal t_{2g} basis functions.

This work presents additional Zeeman spectra measured in luminescence with two magnetic field directions, B||c and B⊥c, and site selective luminescence and excitation spectra. It is now possible to give a microscopic description of the trigonal field in GCrSH and offer an explanation for the difficulty in detecting the second origin $R_2(2\bar{A})$.

Experimental Section

Samples of GAlSH:Cr(III) 2% were prepared as described in the literature.[8]

Luminescence spectra were excited by a Spectra Physics 171 Ar^+ laser, and the luminescence was dispersed by a 0.85 m double Spex 1404 monochromator with 1200 grooves/mm gratings blazed at 750 nm. The excitation spectra were measured by a stepper motor/computer-controlled Spectra Physics 375 dye laser pumped by the SP 171 Ar^+ laser and using DCM in ethylene glycol/propylene carbonate, 3:2.

Samples were cooled either by the flow tube technique or in a 5 T cryomagnet (BOC).

Results

Figure 1 compares the nonselectively excited luminescence spectrum of GAlSH:Cr(III) with the polarized selective excita-

* Corresponding author. E-mail: h-riesen@adfa.edu.au. Fax: ++61 2 6268 80 17.

(1) Holden, A. N.; Merz, W. J.; Remeika, J. P.; Matthias, B. T. *Phys. Rev.* **1956**, *101*, 962.
(2) Burns, G. *Phys. Rev.* **1961**, *123*, 1634.
(3) Lingafelter, E. C.; Orioli P. L.; Schein, B. J. B.; Stewart, J. M. *Acta Crystallogr.* **1966**, *20*, 451.
(4) Schein, B. J. B.; Lingafelter, E. C.; Stewart, J. M. *J. Chem. Phys.* **1967**, *47*, 5183.
(5) Schein, B. J. B.; Lingafelter, E. C. *J. Chem. Phys.* **1967**, *47*, 5190.
(6) Brunetière, F. *Compt. Rend.* **1962**, *255*, 3394.
(7) Martin-Brunetière, F.; Couture, L. *Compt. Rend.* **1963**, *256*, 5327.
(8) Carlin, R. L.; Walker, I. M. *J. Chem. Phys.* **1967**, *46*, 3921.
(9) Tamatani, M.; Ban, T.; Tsujikawa, I. *J. Phys. Soc. Jpn.* **1971**, *30*, 481.

10.1021/ic991465x CCC: $19.00
Published on Web 04/27/2000

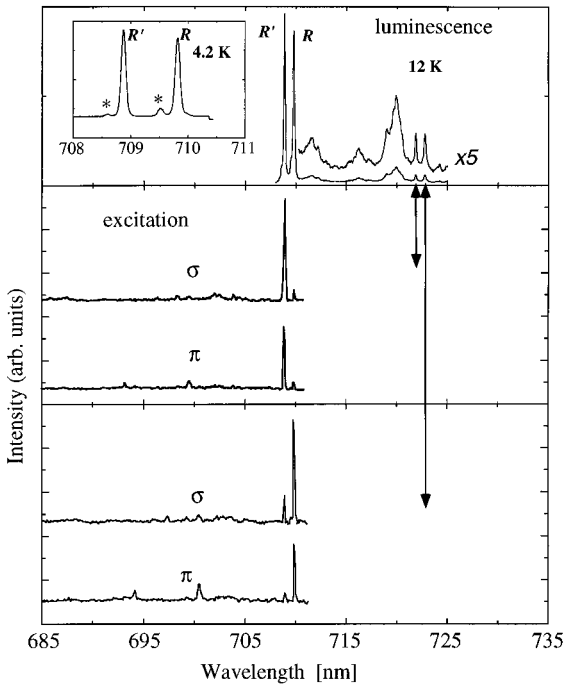

Figure 1. Luminescence and selective excitation spectra of GAlSH: Cr(III) in the region of the $^2E \leftarrow {}^4A_2$ transitions at 12 K. The luminescence was nonselectively excited by 50 mW all-lines Ar^+ laser light. The propagation direction of the laser light was in the (*a*,*b*) plane of the crystal with the electric vector E||c (π) and E⊥c (σ) for the polarized excitation spectra. The vibrational sidelines used to selectively monitor the luminescence for the excitation spectra are indicated by arrows. The inset shows the luminescence spectrum in the region of the electronic origins at 4.2 K. Asterisks denote minority sites.

tion spectra at 12 K. The inset shows the luminescence spectrum in the region of the electronic origins at 4.2 K. Table 1 summarizes the theoretical dipole strengths that are analyzed in detail in the Discussion section. In ref 8 the electronic origins *R* and *R*′ in the absorption spectrum have been interpreted as the R_1 and R_2 lines, respectively, of one hexaaqua species. The intensities of *R* and *R*′ are the same in the 12 and 4.2 K luminescence spectra (Figure 1), and they are comparable to the relative intensities observed in the absorption spectrum of neat GCrSH. The populations of excited-state levels in coordination compounds are usually governed by a pseudo-Boltzmann distribution; that is to say the R_1 and R_2 level thermalize within a fraction of the lifetime of the excited state. The energy difference between *R* and *R*′ is ~19 cm^{-1}. The population of the R_2 level would decrease by a factor *p*:

$$p = \exp\left[-\frac{\Delta E}{k}\left(\frac{1}{T_1} - \frac{1}{T_2}\right)\right] \qquad (1)$$

where $\Delta E = 19$ cm^{-1}, *k* is the Boltzmann factor, and $T_1 > T_2$. This would correspond to $p = 69$ when the temperature is changed from 12 to 4.2 K. Hence the transition *R*′ should be very weak in the 4.2 K spectrum and rather intense in the 77 K spectrum if it was the R_2 line of one site. The absence of such a temperature dependence indicates that the two lines *R* and *R*′ are the R_1 lines of the two crystallographic sites with C_3 and C_{3v} symmetry, in accord with an earlier assignment. This conclusion is fully supported by the selective excitation spectra shown in the lower panels of Figure 1. Nonresonant monitoring of vibrational side lines in luminescence at 721.95 and 722.85 nm renders a high selectivity. The selectivity is not complete due to some partial overlap of vibration side lines.

(10) Manoogian, A.; Leclerc, A. *J. Chem. Phys.* **1975**, *63*, 4450.

Table 1. Dipole Strengths for the $^2E(R_1,R_2) \leftarrow {}^4A_2$ Transitions[a]

	$R_1(\bar{E})$	$R_2(2\bar{A})$
$\alpha(E_x,H_x)$	$1/3\sigma + 1/2\sigma_0 + 192$	$1/3\sigma + 1/6\sigma_0 + 107$
$\sigma(E_x,H_z)$	$1/3\sigma + 1/2\sigma_0 + 5$	$1/3\sigma + 1/6\sigma_0 + 19$
$\pi(E_z,H_x)$	$1/3\pi + 192$	$\pi + 107$

[a] The numbers are the magnetic dipole strength in units of 10^{-4} μ_B^2, calculated from the full d^3 ligand field matrix with $B = 700$ cm^{-1}, $C = 3260$ cm^{-1}, $\Delta = 18000$ cm^{-1}, $\zeta = 220$ cm^{-1}, $k = 0.75$, $v = 2605$ cm^{-1}, and $v' = 386$ cm^{-1} for species $C_{3v}(1)$ (parameters taken from ref 15). σ, σ_0, and π are the third-order electric dipole strengths for the $^2E^a \leftarrow {}^4A_2$ transitions in trigonal symmetry.

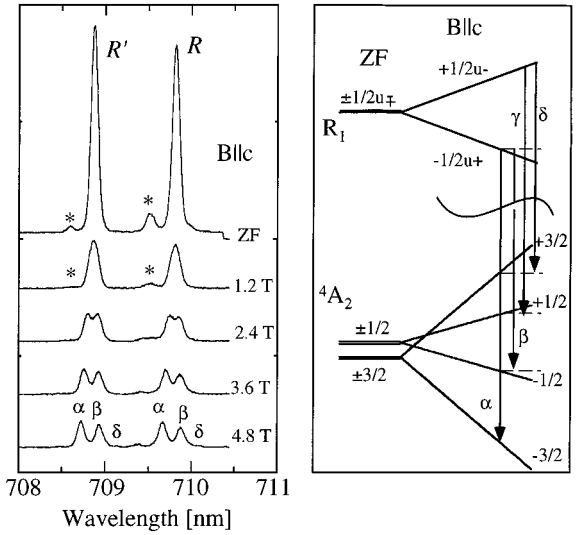

Figure 2. Zeeman effect on the R_1 line in luminescence of GAlSH: Cr(III) with B||c at 4.2 K. The luminescence was excited by 50 mW of all lines of an Ar^+ laser propagating along the direction of the magnetic field *B*. The luminescence was observed also along *B* in a *f*/1 geometry. The diagram shows the calculated energy pattern for $D(^4A_2) = 0.18$ cm^{-1} for a field range of 0−1 T.

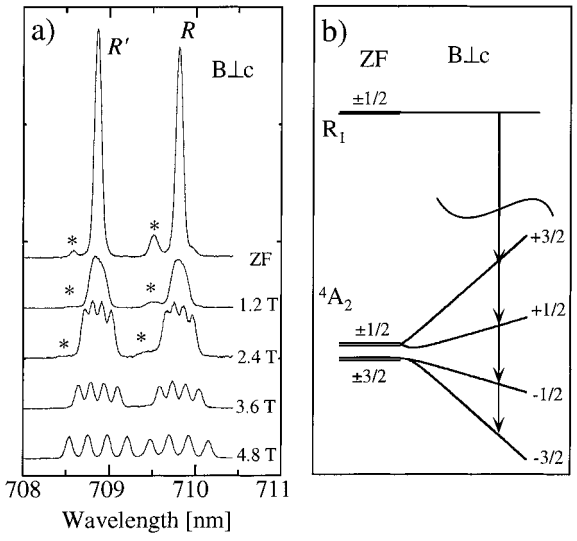

Figure 3. As in Figure 2 but with B⊥c.

The Zeeman effect on the transitions *R* and *R*′ in luminescence are displayed in Figures 2 and 3 for the magnetic field **B** parallel, B||c, and perpendicular, B⊥c, to the crystal *c* axis. The excited states for the (t_2^3) ^2E multiplet are $|2\bar{A}\pm\rangle = |\pm 1/2u\pm\rangle$ and $|E\pm\rangle = |\mp 1/2u\pm\rangle$, where $|u\pm\rangle$ are the complex trigonal basis functions for the cubic E representation. Four transitions with

Table 2. Dipole Strengths for the Axial Zeeman Spectrum of the $R_1(\bar{E})$ Line[a]

$M_S{}^{z\,b}$	$\lvert\bar{E}+\rangle = \lvert-1/2u+\rangle$	$\lvert\bar{E}-\rangle = \lvert+1/2u-\rangle$
+3/2		$1/4\sigma_0 + 57$ (δ)
+1/2		$1/6\sigma + 39$ (γ)
−1/2	$1/6\sigma + 39$ (β)	
−3/2	$1/4\sigma_0 + 57$ (α)	

[a] This table applies to Figure 2, where the measured dipole strengths are $D^x_z(z) + M^y_z(z)$. For $D^\alpha_\beta(\gamma)$ and $M^\alpha_\beta(\gamma)$, γ is the direction of light, β is the direction of the applied magnetic field, and α is the direction of the electric and magnetic vector of light for D and M, respectively. The numbers (magnetic dipole strengths) are defined in Table 1 and were calculated by diagonalizing the d^3 ligand field matrix with $B = 4.8$ T applied along the molecular trigonal z axis. [b] The ground-state spin functions are quantized along the trigonal z axis

$\Delta M_J = \pm 1$ are expected for the geometry B||c (Figure 2). The ground state, $|M_s{}^{gr}\,{}^4A_2\rangle$ has $M_J{}^{gr} = M_s{}^{gr}$. The components of the effective angular momentum of the excited state $|M_s{}^{ex}u\pm\rangle$ are $M_L{}^{ex} = \pm 1$ and $M_J{}^{ex} = M_s{}^{ex} + M_L{}^{ex}$. In trigonal symmetry $\Delta M_J = \pm 1$ is equivalent to $\Delta M_J = \mp 2$. The four transitions shift by

$$\Delta E = \mu_B(M_J{}^{ex} g_{||} - M_J{}^{gr} g) B_z \qquad (2)$$

where the isotropic g value of the ground state is $g = 1.98$, and μ_B is the Bohr magneton.

In 4.8 T the excited-state splitting is substantial, ≈ 7 cm^{-1}, and hence the population of the excited-state level $|\bar{E}-\rangle = |+1/2u-\rangle$ is only about 1/10 of the population of the $|\bar{E}+\rangle = |-1/2u+\rangle$ level. Hence, the intensities of transitions γ and δ are expected to be about 10 times weaker in comparison with transitions α and β. Thus the two prominent lines in the 4.8 T spectrum are assigned to α and β. Transition δ can also be identified at the lower energy side of β. However, transition γ overlaps with the more intense transition α and is therefore not visible in the present spectra. In the 4.8 T spectrum the transitions α, β shift by 3.08 cm^{-1}, −1.17 and 2.91 cm^{-1}, −1.17 cm^{-1} with respect to the zero field positions of R and R', respectively. α is slightly more intense than β. Thus we can conclude that in zero field the intensities of the transitions to the $\pm 1/2$ and $\pm 3/2$ Kramers doublets are approximately the same since with B||c there is no mixing of these spin levels. Hence the energy of R and R' in zero field would correspond to the average transition frequency. This has to be taken into account when evaluating the $g_{||}$ value. In particular half of the ZFS has to be subtracted or added to the observed shift for α and β, respectively. The theoretical dipole strengths for the axial Zeeman spectra (Figure 2) are summarized in Table 2.

By using eq 2 the $g_{||}$ value can be evaluated from the data points. We obtain $g_{||} = -3.1$ and $g_{||} = -3.2$ for R and R', respectively. This is in good agreement with the values of 3.14 and 3.15 obtained in the early work of ref 7. The sign of $g_{||}$ is defined by the symmetry transformations of $|\bar{E}\pm\rangle$ and the selection rules given in Tables 1 and 2.

The $R_1(\bar{E})$ lines display virtually no splitting or shift in the experiment with B⊥c illustrated in Figure 3, and the observed pattern of four lines reflects only the splitting in the $^4A_2$ ground state. The theoretical dipole strengths for this geometry are given in Table 3. When B⊥c the magnetic field couples the R_2 and R_1 lines and the R_1 line is expected to shift by[11]

$$\Delta E(R_1) = -g_\perp{}^2 \mu_B{}^2 B^2 / 4E(R_2 - R_1) \qquad (3)$$

where $E(R_2 - R_1)$ is the zero field splitting of the ^2E state. The

Table 3. Dipole Strengths for the Zeeman Spectrum in Figure 3[a]

$M_S{}^x$	$R_1(\bar{E}+,\bar{E}-)^b$
+3/2	$1/2(1/8\sigma + 1/16\sigma_o + 1/8\pi + 42)$
+1/2	$1/2(1/24\sigma + 3/16\sigma_o + 1/24\pi + 53)$
−1/2	$1/2(1/24\sigma + 3/16\sigma_o + 1/24\pi + 54)$
−3/2	$1/2(1/8\sigma + 1/16\sigma_o + 1/8\pi + 47)$

[a] In Figure 3 the dipole strengths measured are $1/2(D^z_x(x) + M^y_x(x) + D^y_x(x) + M^z_x(x))$. The magnetic dipole strengths were calculated for $B = 4.8$ T applied along the x direction. [b] The dipole strengths are summed over the two components of R_1.

Table 4. Ligand Field Calculation for GCrSH[a]

parameter	observed[b]	calculated
$D(^4A_2)$	0.180	0.181
$R_1(\bar{E})$	14 133	14 133
$D(^2E)$		−88
$g_{||}(^4A_2)$	1.975(5)	1.978
$g_\perp(^4A_2)$	1.975(5)	1.977
$g_{||}(\bar{E})$	−3.2	−3.12
$g_\perp(\bar{E},2\bar{A})^c$		1.98
$g'_\perp(\bar{E})$	0.07	0.05
$g_{||}(2\bar{A})$		0.78

[a] All energies in cm^{-1}. [b] EPR data for GGaSH:Cr^{3+} at 4.2 K.[10] Optical data for GCrSH at 4.2 K.[8] [c] $D(^2E) = E(\bar{E}) - E(2\bar{A})$ and $g_\perp(\bar{E},2\bar{A})$ is the g value for the off-diagonal Zeeman term connecting $|2\bar{A}\pm\rangle = |\pm 1/2u\pm\rangle$ and $|\bar{E}\pm\rangle = |\mp 1/2u\pm\rangle$. Other parameters as in Table 1.

$R_1(\bar{E})$ line is also expected to split by $(1/2)g'_\perp \mu_B B$. However, $g'_\perp$ is usually very small (see Table 4). The experiments provide an upper limit for the shift of the R_1 line of 0.1 cm^{-1}. This corresponds to a lower limit for the R line splitting of $E(R_2 - R_1) \geq 50$ cm^{-1}.

Figure 4 shows a comparison of vibrational side lines observed in selective luminescence and excitation spectra in the region 30−300 cm^{-1}. The region of 75−160 cm^{-1} in excitation exhibits enhanced intensity and new lines compared to the luminescence.

Discussion

Transition Dipoles and Polarization Ratios. Carlin and Walker[8] had noted that for GCrSH the α spectra do not correlate with either σ or π spectra. This observation together with the small oscillator strengths, $f \approx 3 \times 10^{-9}$, indicates that the sharp lines in GCrSH and GAlSH:Cr^{3+} have mixed electric and magnetic dipole character. The experimental oscillator strengths refer to a crystal containing only one species of Cr^{3+}. Since R and R', in fact, refer to the $C_3(2)$ and $C_{3v}(1)$ species, the oscillator strengths in ref 8 must be multiplied by 3/2 and 3 for the R and R' lines, respectively.

The ligand field spectrum of GCrSH has much in common with ruby, Al_2O_3:Cr^{3+}. Thus we find the cubic fields $\Delta = 18\,100$ and 18 000 cm^{-1} and the transition energies $E(^2E^a) = 14\,400$ and 14 120 cm^{-1}, and $E(^2T_2{}^a) = 21\,400$ and 22 000 cm^{-1}, for ruby and GCrSH, respectively. The cubic field Δ is defined in eq 4, where $v' = \langle e_{u\pm}|H_{trig}|t_{2x\pm}\rangle$ denotes the off-diagonal trigonal field.

$$\Delta = 10Dq - \frac{1}{\sqrt{2}} v' - \frac{1}{3} v \qquad (4)$$

Equation 4 can be derived from the ligand field analysis given on p 127 in ref 11.

(11) Sugano, S.; Tanabe, Y.; Kamimura, H. *Multiplets of Transition Metal Ions in Crystals*; Academic Press: New York, 1970.

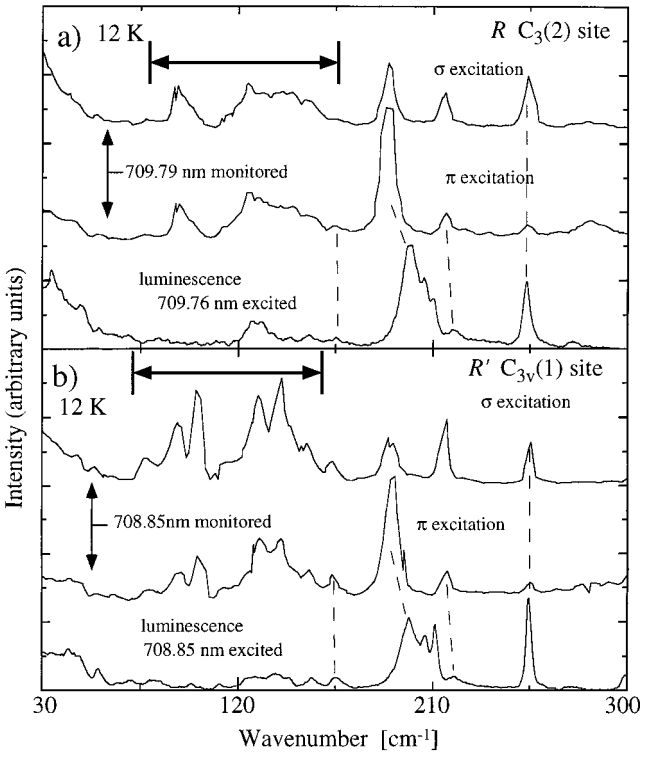

Figure 4. Comparison of vibrational side lines in luminescence and polarized excitation spectra of GAlSH:Cr(III) in the region of the $^2E \leftarrow {}^4A_2$ transition at 12 K. Excitation spectra were monitored with a bandwidth of ~2 Å at 709.79 and 708.85 nm in panel (a) and (b), respectively. The luminescence spectra were excited at 709.76 and 708.85 nm in (a) and (b), respectively. Shifts are relative to the origins.

For ruby, the magnetic dipole contribution is only a minor component of the dipole strength for the R_1 and R_2 lines.[12] It is possible to account for the σ and π polarization ratios by ignoring the small deviation from local C_{3v} symmetry, but it is essential to take into account both $V(T_{1u0})$ and $V(A_{2u})$ odd parity potentials that are permitted in C_{3v} symmetry. Table 1 gives the electric dipole strengths for any trigonal Cr^{3+} complex in terms of the third-order parameters. In ruby, the observed polarizations of the R_1 and R_2 lines can be accounted for by using

$$\pi:\sigma:\sigma_0 \approx 0.10:1.00:0.99 \qquad (5)$$

The principal perturbations in the third-order mechanism ($\bar{\bar{P}}^{\alpha}$) involve spin−orbit mixing and an effective second-order electric dipole operator (($\bar{P}^{\alpha} = V_{odd}P^{\alpha}$) between $^4A_2$, $^2E^a$, $^2T_2{}^a$, $^2T_2{}^b$, and $^4T_2$ states. In C_{3v} symmetry the transition $^4T_2 \leftarrow {}^4A_2$ is forbidden in π for a static electric dipole mechanism. The observed π intensities for this transition must come from either a magnetic dipole or vibronically induced electric dipole mechanism. The latter does not contribute π intensity to the zero phonon R_1 and R_2 lines.[12]

The R_1 and R_2 lines can get electric dipole π intensity from the perturbation process[13]

$$^2E^a \xleftarrow{\bar{P}^{\alpha}} {}^2T_2{}^a \xleftarrow{H_{so}} {}^4A_2$$

This mechanism is evidently weak for ruby. It is also weak for Cr^{3+}:$LiNbO_3$ and Cr^{3+}:$LiTaO_3$,[14] which contain the relatively rare C_{3v} site. Consequently we infer that the π/σ and π/σ_0 ratios are small for all Cr^{3+} ions in C_{3v} sites, provided the observed lines are predominantly electric dipole.

In ruby $f\sigma/f\pi \approx 18$ for $R_1(\bar{E})$, but for GCrSH $f\sigma/f\pi \approx 1.7$. Table 1 provides the solution for the dramatic difference in the polarization ratios. The magnetic dipole strength for the $R_1(\bar{E})$ line in π is $192 \times 10^{-4}\ \mu_B{}^2$ and corresponds to an oscillator strength of 8.2×10^{-9}. This number may be reduced by electron−phonon coupling by as much as a factor of 2. Even so, comparison with the experimental values indicates that most of the π oscillator strength is magnetic dipole and the σ oscillator strength is nearly all electric dipole. The intensity distributions in Figures 2 and 3 can be followed by using calculated dipole strengths, given in Tables 2 and 3. Figures 1−3 are not suitable for an accurate ratio of π/σ, but we estimate that

$$\pi:\sigma:\sigma_0 \approx 0.1:1.00:0.65$$

for the R_1' line in GAlSH:Cr^{3+}.

Microscopic Model for the Trigonal Fields. The large value of $|g_{||}| = 3.2$ and the absence of any shift for the R_1 lines in the B⊥c experiment give direct evidence for a very large v trigonal field.[11] The sign of v is readily deduced from the X-ray structure. Both the C_{3v} and the C_3 complex ions are closely related in structure as well as in the optical and EPR spectra. The precise analysis for the geometric parameters is more complicated for the C_3 ion, and we will examine in detail only the higher symmetry C_{3v} species.

The X-ray structure of GCrSH[4] shows that the OH_2 ligands are rotated in the same sense as in β alums.[15] In fact, the C_{3v} symmetry demands that they are rotated by $\omega = -45°$, where ω is defined to be the anticlockwise rotation of OH_2 about the CrO bond. The microscopic model for trigonal ligand fields in alums[15] can be applied directly to GCrSH. A schematic diagram defining the angles ω and t is given in ref 15.

Consider an OH_2 ligand bound to a Cr^{3+} ion. If any small differences in the OH bonds are neglected, then both planar and pyramidal OH_2 ligands will have a local plane of symmetry labeled y that contains the lone pair of the oxygen atom. By using the angular overlap model (AOM)[16] one can derive for $Cr(OH_2)_6{}^{3+}$ an approximate formula for v:

$$v = -3\sin(2\omega)(e_{\pi y} - e_{\pi x}) - 3\sqrt{2}d(\theta)(e_{\pi y} + e_{\pi x}) \qquad (6)$$

where $d(\theta) = (\theta - \theta_{O_h})\pi/180$ and θ is the angle between the CrO vector and the molecular trigonal z axis. There is no trigonal twist in alums and in GCrSH. $e_{\pi x}$ represents the π perturbation of the metal d orbitals by the "saturated" part of the OH_2 ligand. $e_{\pi y}$ contains the π perturbation by the unsaturated lone pair and should be much larger than $e_{\pi x}$.

In the conventional ligand field model trigonal anisotropy in spin−orbit coupling is neglected and the ZFS is mainly determined by the off-diagonal trigonal field.[17]

One can use the AOM model to derive an approximate formula for v':[15]

$$v' = 3d(\theta)e_{\sigma} - \frac{\sqrt{6}}{2}[\cos(\omega) - \sin(\omega)]e_{\sigma\pi}(t) \qquad (7)$$

The second term vanishes for planar OH_2 ligands. The lone pair on the oxygen atom may be approximated as a tilted pπ orbital and as a tilted dipole. If the small admixture of s orbitals is

(12) Nelson, D. F.; Sturge, M. D. *Phys. Rev.* **1965**, *137*, A1117.
(13) Dubicki, L. Unpublished work.
(14) Glass, A. M. *J. Chem. Phys.* **1969**, *50*, 1501.
(15) Dubicki, L.; Bramley, R. *Chem. Phys. Lett.* **1997**, *272*, 55.
(16) Schäffer, C. E. *Struct. Bonding* **1968**, *5*, 68.
(17) MacFarlane, R. M. *J. Chem. Phys.* **1967**, *47*, 2066.

Table 5. Geometric Parameters for $Cr(OH_2)_6^{3+}$ Ions in GCrSH at 295 K[a]

	R(CrO) (Å)	θ (deg)	t (deg)
C_{3v} top $Cr(O7)_3$	1.934	56.9	−18
C_{3v} bottom $Cr(O8)_3$	1.966	55.5	0
C_3 top $Cr(O10)_3$	1.935	56.3	0
C_3 bottom $Cr(O11)_3$	1.984	55.9	−15

[a] The notation of the oxygen atoms follows ref 4. The tilt angles for $Cr(O8)_3$ and $Cr(O10)_3$ are ∼2° and ∼5°, respectively, and are not significant.

neglected, then $e_{\sigma\pi}(t)$ is proportional to $\sin(2t)$. Note that

$$e_{\sigma\pi}(-t) = -e_{\sigma\pi}(t) \tag{8}$$

where the tilt angle t is defined to be positive if the lone pair is tilted away from the positive direction of the cubic axes.[15] For α alums we find that $e_{\sigma\pi}(18°) \approx -380$ cm^{-1}. The ZFS in GMSH:Cr^{3+} is sensitive to temperature and to the size of the M^{3+} ion. Since the X-ray structure[4] of GCrSH was performed at 295 K and the ionic radii of Cr^{3+} and Ga^{3+} are similar, we must use $D(^4A_2) = 0.114$ cm^{-1} for the C_{3v} ion in GGaSH:Cr^{3+} at 295 K.[10] The data in Table 4 and the relationship derived from ligand field theory,[17] $D(^4A_2) \propto \zeta^2 v'$, can be used to derive $v' \approx 240$ cm^{-1} for GGaSH:Cr^{3+} at 295 K.

If the ligands in GCrSH are planar, then v' should be determined by e_σ and the cone angles θ. Such a calculation leads to $v' \approx 600$ cm^{-1}, which is in serious disagreement with the value of 240 cm^{-1} derived above. It is therefore essential to determine whether the OH_2 ligands are pyramidal.

The hydrogen atom coordinates in the X-ray structure are not accurate enough for calculating tilt angles. However, Table 8 in ref 4 shows that just like alums, GCrSH is a rare case where all the OH_2 ligands form very strong H-bonds with O···O distances in (O−H···O) ranging from 2.6 to 2.66 Å. Such short H-bonding should be linear, and we can use the oxygen atoms to determine the tilt angles.[18] The results are summarized in Table 5. The Cr−O bond distances in alums are fairly constant, and we take 1.96 Å as the standard value. It is well established[19] that the cubic ligand field has a distance dependence $\Delta \propto 1/R$.[5] Since Δ is largely determined by e_σ, $\Delta = 3e_\sigma - 2e_{\pi x} - 2e_{\pi y}$, we assume that e_σ and, for simplicity, all the remaining AOM parameters have the same distance dependence. One can calculate, for example, $e_\sigma(1.934\ Å) = e_\sigma(1.96\ Å) \times 1.069$.

Equations 6 and 7 are approximate. The exact expressions can be determined by using the AOM matrices.[16] Following earlier work[15] we transform $e_{\pi x}$ and $e_{\pi y}$ into the isotropic $\pi^e = e_{\sigma x}$ and anisotropic component $\pi^o = e_{\pi y} - e_{\pi x}$ and assume that $\pi^o(t) \approx \pi^o \cos^2(t)$ and π^e is independent of t. All the AOM parameters are normalized to the standard 1.96 Å Cr−O distance, and the separate calculations for the top CrO_3 and bottom CrO_3 are added to give

$$\Delta = 3.068e_\sigma - 4.091\pi^e - 1.940\pi^o$$

$$v = 0.0073e_\sigma - 0.234\pi^e + 2.708\pi^o + 0.084e_{\sigma\pi}(-18°)$$

$$v' = 0.0819e_\sigma - 0.078\pi^o - 0.966e_{\sigma\pi}(-18°) \tag{9}$$

The cubic field $\Delta \approx 18\,000$ cm^{-1} and $\pi^o = 1000$ cm^{-1} are taken from ref 15. Estimates of the π^e parameter are less accurate. If $\pi^e = 0$, then $e_\sigma \approx 6500$ cm^{-1}. If $\pi^e \approx 1000$ cm^{-1} ($e_{\pi x} = 1000$ cm^{-1} and $e_{\pi y} = 2000$ cm^{-1}), then $e_\sigma \approx 8000$ cm^{-1}. We have some evidence from the spectroscopy of alums and trigonal metal hexaammine complexes that π^e may be as large as 1000 cm^{-1}.[13] We choose $\pi^e = 750$ cm^{-1} and hence $e_\sigma = 7500$ cm^{-1}. Equation 9 gives

$$v' = 614 - 78 - 367$$

$$\approx 170\ \text{cm}^{-1}$$

which compares fairly well with the ligand field value of $v' = 240$ cm^{-1}. The remaining discrepancy may be due to small differences in the geometry parameters of the impurity ion $Cr(OH_2)_6^{3+}$ to that of the GGaSH host, to some contribution of anisotropic spin−orbit coupling, $\zeta_z \neq \zeta_x$, to $D(^4A_2)$, and to errors in our chosen set of AOM parameters.

Note that eqs 6 and 7 are approximate and are derived by decoupling the effects of rotation (ω) and displacement (θ). The small deviations from the approximate equations, $\nu' \approx \nu'(\theta) + \nu'(\omega,t)$ and $\nu \approx \nu(\omega) + \nu(\theta)$, are indicated in eq 9. Also, the contribution to v' from pyramidality has a negative sign, the same sign as found in α alums.[15] This is a consequence of two sign changes, one in tilt and the other in the angular factor containing ω. For α alums, $\omega = 90°$ and eq 7 gives

$$v'(\omega,t) = \frac{\sqrt{6}}{2} e_{\sigma\pi}(t) \tag{10}$$

where t is positive and $e_{\sigma\pi}(18°) \approx -380$ cm^{-1}. For GCrSH, $\omega = -45°$ and for three tilted OH_2 ligands

$$v'(\omega,t) = -\sqrt{3}/2e_{\sigma\pi}(-18°) = +\sqrt{3}/2e_{\sigma\pi}(18°) \tag{11}$$

Finally, eq 9 gives

$$v = 55 - 176 + 2740 + 32$$

$$\approx 2650\ \text{cm}^{-1}$$

Such a large value for v is consistent with the observed large $g_{||}(\bar{E})$ (see Table 4) and the absence of any shift of the R_1 line for the B⊥c experiment. It is in fact an obvious consequence of $\omega = -45°$, which is one of the optimum angles for maximizing the magnitude of v.

Nature of the R_2 Line. Comparison between the selective luminescence and excitation spectra (Figure 4) indicates new absorption lines in the range 75−160 cm^{-1}. The multiplicity of new lines in excitation suggests that the second origin $R_2(2\bar{A})$ is more strongly vibronically coupled than $R_1(\bar{E})$ and that the coupling involves several different vibrations. This problem appears to be similar to that observed in β alums, CsTiSH.[20,21] The large trigonal splitting should be modulated most strongly by the "external" twisting vibration of the OH_2 ligand.[20] In the local C_{3v} symmetry of the $M(OH_2)_6^{3+}$ complex the A+E combinations of the twist vibration will couple to some degree with the low-frequency skeletal modes $\nu_5(T_{2g})$ and $\nu_6(T_{2u})$. Furthermore, the strong H-bonding between OH_2 ligands and

(18) Beattie, J. K.; Best, S. P.; Del Favero, P.; Shelton, B. W.; Sobolev. A. N.; White, A. H. *J. Chem. Soc., Dalton Trans.* **1996**, 1481.
(19) Hitchman, M. A. *Inorg. Chem.* **1982**, *21*, 821.
(20) Tregenna-Pigott, P. L. W.; O'Brien, M. C. M.; Pilbrow, J. R.; Güdel, H. U.; Best, S. P.; Noble, C. *J. Chem Phys.* **1997**, *107*, 8275.
(21) Dubicki, L.; Riley, M. *J. Chem. Phys.* **1997**, *106*, 1669.

the O atoms of the SO_4^{2-} ions will couple the twist with low-energy lattice modes. The distribution of the $R_2(2\bar{A})$ electronic character will become a multimode vibronic problem. The vibronic activity of the $^2E(t_2^3)$ is under investigation.[22]

Conclusions

GCrSH has a very large trigonal field $v \approx 2600$ cm^{-1}. This result is consistent with the small ZFS[23] $D(^3A_2) = 3.74$ cm^{-1}, observed for GAlSH:V^{3+} (d^2). It also provides a solution[22] for the complicated EPR spectrum[23] observed for GAlSH:Ti^{3+} (d^1). The GAlSH lattice closely resembles the β alum, CsAlSH, both in the H-bonding of the OH_2 ligands and in the presence of a large v.

The absence of a prominent R_2 line is also observed in other complexes such as the β alum CsCrSH (d^3). This feature appears to be a consequence of the large trigonal field, v, and its modulation by vibrations, in particular by lattice modes.

IC991465X

(22) Dubicki, L.; Riley, M. Unpublished work.
(23) Schwartz, R. W.; Carlin, R. L. *J. Am. Chem. Soc.* **1970**, *92*, 6763.